RESEARCH ARTICLE

Performance Evaluation of Multi-Hop LoRaWAN

MD. RAKIBUL ISLAM[1], **MD. BOKHTIAR-AL-ZAMI**[1], **BISWAJIT PAUL**[1],
RAJESH PALIT[2], **(Member, IEEE), JEAN-CHARLES GRÉGOIRE**[3],
AND SALEKUL ISLAM[4], **(Senior Member, IEEE)**

[1]Department of Electrical and Electronic Engineering, Shahjalal University of Science and Technology, Sylhet 3114, Bangladesh
[2]Department of Electrical and Computer Engineering, North South University, Dhaka 1229, Bangladesh
[3]Institut National de la Recherche Scientifique (INRS), Université du Québec, Montreal, QC H2L 2C4, Canada
[4]Department of Computer Science and Engineering, United International University, Dhaka 1212, Bangladesh

Corresponding author: Salekul Islam (salekul@cse.uiu.ac.bd)

ABSTRACT Although LoRa (radio) technology offers customization of different physical layer transmission parameters such as bandwidth, spreading factor (SF), transmission power, and coding rate to obtain the desired data rate and coverage, the currently preferred single-hop transmission mode cannot simultaneously achieve both. The LoRaWAN community is therefore focusing on multi-hop networks to increase network longevity while extending coverage. In this paper, a detailed mathematical model for a multi-hop network that modifies the Distance Ring Exponential Stations Generator (DRESG) framework is presented. The relay operation is carried out through intermediate gateways, and a distance-based adaptive transmission configuration approach is used. On the basis of the performance metrics, i.e., packet delivery ratio (PDR) and energy usage of end nodes, we compare and contrast the performance characteristics of several routing schemes, including single-hop (SH), next-ring-hop (NRH), and variable-hop (VH) routing. The research covers some core issues, including interference, environmental conditions, and transceiver power constraints, and sets the stage for evaluating various multi-hop LoRa solutions as well as optimizing several implementation factors.

INDEX TERMS Energy efficiency, interference, LoRaWAN, packet delivery rate, routing.

I. INTRODUCTION

The Internet of Things (IoT) promises to facilitate interconnection and collaboration across various types of devices to provide smart services for various environments in a seamless manner [1]. There will be billions of IoT devices in use over the next several years, allowing for the development of smart systems for a variety of purposes, including smart cities, farms, hospitals, factories, and transportation systems, among many others [2]. Whether in a city, a building, or a farm, these applications are not feasible without wireless networks. ZigBee, Bluetooth, and Wi-Fi are the three most common wireless technologies employed for this purpose, and all have a limited range. Low-Power Wide Area Networks (LPWANs) are now used in many IoT deployment scenarios, which have wider coverage, low operating costs, and long battery life in

end devices. They use the unlicensed sub-1GHz industrial, scientific, and medical (ISM) frequency spectrum to send short packets at slow data rates, reducing exploitation costs. Therefore, it is anticipated that LPWANs will be appropriate for supporting IoT services, which demand modest data throughput and broad coverage.

The deployment density, whether sparse or dense, varies depending on the specific application scenario. Numerous real-world applications require the deployment of dense LoRa networks. The LoRa Alliance claims that 1 million connected devices are now part of the LoRaWAN. The LoRaWAN network design makes it simple and affordable to expand wireless network coverage without disrupting the network. This design enables the network to be scaled as needed to meet the requirements of any given application or environment. For instance, Smart Harbors implemented 1000 nodes for asset and vehicle tracking [3]. In [4], the author demonstrated the application of LoRaWAN in the

flower industry, where numerous trolleys needed to be connected to a server while moving around an auction floor space, and the ability of a single gateway to support as many as 6,000 nodes (trolleys). Furthermore, LoRa technology is being studied for the deployment of industrial wireless networks suited for sensors and actuators of the Industry 4.0 era, and it has been experimentally demonstrated that with proper planning of time, frequency, and spreading factors, up to 6,000 nodes can be accessed up to one minute cycle time [5]. Massive scale evaluations of LoRa technology for indoor remote health and wellbeing monitoring and vehicle communication are also presented in [6] and [7]. Real-world industrial deployments have also benefited from LoRa technology and improved business efficiencies. For example, Enthu Technology Solutions India Pvt Ltd and Xorowin Mechatronics recently collaborated with Semtech to develop SIPOAL (Self-Powered Electromechanical Controller) [8]. It is an Internet of Things (IoT)-based smart single-point lubricator and self-powered electromechanical controller that automatically provides the right amount of lubricant to machines at user-programmed intervals. For IT and Operational Technology (OT) environments, Cisco created new IoT sensor solutions employing LoRaWAN to improve visibility into physical locations [8]. This sensor uses the LoRaWAN protocol to wirelessly connect the battery-operated Internet of Things. For better logistics, theft prevention, and operational efficiency, gateways utilizing the LoRaWAN protocol allow geolocation capabilities to track and monitor asset locations. In addition, LoRa-enabled sensors from Transco can be seamlessly integrated into existing mining infrastructure, such as conveyor belts [8]. These compact, long-lasting sensors communicate with private networks using the LoRaWAN technology, which enables the constant transmission of real-time data despite the harsh conditions underground. Recently AIUT LLC. (a hardware and software company specializing in Internet of Things (IoT)-based solutions in the oil and gas markets) uses Semtech's LoRa devices and the LoRaWAN protocol to deliver reliable, continuous, and remote LPG monitoring and deployment flexibility [8].

LoRaWAN has been developed to meet the large area coverage and low data rate requirements of IoT-based services. In a LoRaWAN network, a star topology is used by end devices to connect with gateways [9], [10], [11], [12]. It has been discovered that LoRaWAN, especially in open areas and rural settings, has a potential range of several kilometers. However, this performance will be poorer in areas with impediments like buildings or mountains. In congested networks, interference and packet collisions also reduce performance. The energy usage of the network consequently rises as its dependability falls. Although the LoRaWAN specification only stipulates a single-hop between end devices and the gateway [13], [14], [15], various studies have proposed multi-hop solutions for network extension or improvements [2], [16], [17], [18], [19], [20], [21], [22], [23], [24], [25], [26], [27], [28], [29], [30], where some devices operate

as relays, routers, or intermediate gateways. Most commonly, multi-hop communication is employed to increase battery life and network longevity by optimizing the wireless network energy consumption and increasing the coverage. Other research work has proposed multi-hop routing to address scalability, capacity, and reliability issues in LoRaWAN networks [31], [32]. The majority of recent research on multi-hop LoRaWAN has dealt with either real-life deployments of such networks or network models that include relay nodes or router nodes [2], [16], [17], [18], [19], [20], [21], [22], [23], [24], [25], [26], [27], [28], [29], [30]. In this article, we present a model to compare and contrast single-hop and multi-hop networks. The use of intermediate gateways is considered in multi-hop settings. We provide examples of how our model benefits LoRaWAN networks. The findings offer fresh perspectives on LoRaWAN multi-hop designs.

The main contributions of this paper follow:

1) A detailed mathematical framework is developed for the realization of a multi-hop LoRaWAN system. This permits the optimization of different parameters of this system.
2) Further, this framework is adaptable to incorporate any transceiver and path loss models. As a result, it establishes a context for assessing the system's effectiveness in user-specified situations.
3) We study the performance of Multi-Hop LoRaWAN and asses its potential benefits through the analysis of representative LPWAN scenarios. Various interference issues such as inter-SF interference, intra-SF interference, co-channel interference, and transceiver's power limitations are considered.
4) Finally, to reduce device energy consumption and lengthen network lifetime, we have devised an adaptive energy-saving strategy that allows the transceiver module to select the best configuration when delivering a packet to its next destination. Since node and gateway locations are known, the device selects the appropriate configuration (transmission power, current, spreading factor) based on its distance from the receiver.

The remaining sections of the paper are organized as follows: different related work pertaining to multi-hop are summarized in section II. A description of the proposed system model is provided in section III. An extensive mathematical model for the proposed multi-hop LoRaWAN system is presented in section IV. Section V presents our evaluation framework, including the algorithms we have developed. In section VI, the system performance is evaluated, and analyses are presented. Finally, the paper is concluded in section VII.

II. LITERATURE REVIEW
A. RELATED WORK
LPWANs have emerged in recent years as a practical solution for applications needing extensive range and low power consumption [33]. LoRaWAN technology ensures long-distance

TABLE 1. Comparison among various multi-hop LoRaWAN approaches.

Refs.	Objective	Applications	Mathematical model	Studied parameters	Limitations
Experiment-based research					
[2]	Employed LoRaWAN mesh in IoT wide-area network to evaluate performance. Mesh devices were set up around campus.	Indoor and outdoor IoT application	Not provided	Impact of node numbers, distances, SF settings, and number of hops on PDR	Simultaneous transmission is not implemented, impact of interference is not studied.
[16]	Employed an underground monitoring system. An ad-hoc transmission technique optimized the node's wake-up time to reduce power usage.	Underground IoT applications	Used some derived equations to analyze data from experiments	Battery capacity dependency on the node number during time synchronization.	No insight into interference, retransmission, and acknowledgment.
[17]	Proposed to link subsurface sensors to an existing LoRaWAN using synchronous LoRa mesh. Enhanced data quality and consistency.	Underground IoT applications	Examined data by using some derived equations	Analysis of Lora-mesh packet error rate, both with and without relay node.	Maximum number of child nodes is limited, no analysis of energy consumption.
[18]	Proposed a multi-hop routing protocol for LoRa mesh networking with both theoretical and experimental results	Large rural sensor networks and urban IoT deployment	Not provided	Demonstrated route construction times based on intermediate gateway and hop numbers, and delay.	No insight into successful reception of packets, energy consumption, and throughput.
[19]	Designed, developed, and integrated TSCH-over-LoRa into TSCH/6TiSCH networking stack of Contiki-NG operating system.	Indoor and outdoor IoT application	Not provided	Investigated the system's dependability (PDR) and radio duty cycle (a proxy for energy consumption)	Not enough insights regarding multi-hop and TDMA-LoRa conjunction.
Simulator based research					
[20]	Introduced JMAC, a multi-hop protocol for smart cities and industry. JMAC uses wireless networks' mesh nature to improve coverage.	Outdoor IoT applications	Provided mathematical model for JMAC	PDR, end-to-end delay and throughput were measured in terms of child nodes	No theoretical analysis of JMAC's performance in LoRa's physical modulation and signal collision model.
[21]	Proposed a multi-hop protocol and SDN-based extension to match LoRa's PHY layer coverage, maximize coverage, and lower energy use.	Outdoor IoT application	Provided algorithm for layer formation, gateway discovery, and forwarding paths construction.	Packet reception ratio (PRR) and network energy consumption depending on node density	Did not study how relay node and area radius affect packet reception ratio and energy consumption.
Analytical model based work					
[22]	Developed a mathematical model to generalize multi-hop behavior. Relay nodes reduced energy consumption, enhanced packet delivery and throughput.	Indoor and outdoor IoT applications	Developed mathematical model.	Investigated energy consumption, throughput, delay, and packet delivery ratio of single- and multi-hop relay networks.	Relay's battery depleted faster for heavy traffic, causing network separation and limiting smart features.
[23]	Explored the influence of multi-hop uplink on LPWAN energy consumption, where nodes transmit packets at low power and high data rates to adjacent parent nodes.	Indoor and outdoor IoT application	Provided a mathematical model for DRESG to evaluate optimal-hop routing.	Compared energy consumption for various ring distance spreading models to find the optimal ring-hop combination	Did not study interference issues and retransmission.
[24]	Proposed a scalable and energy-efficient solution (SEES) for green IoT wireless nodes. Studied the impact of energy-harvesting strategies by using ambient energy-harvesting relay nodes.	Smaller sensor data collection	Presented a mathematical model of the systems and provided an algorithm for the processes.	Analyzed nodes' longevity, energy cost and gain of the nodes, and throughput.	Did not study interference, and the system is not compatible with LoRaWAN features.
[Our work]	Lay out a comprehensive and flexible framework to evaluate multi-hop LoRaWAN's performance considering key performance metrics like packet delivery ratio and energy consumption. Determine the most suitable routing scheme for different deployment scenarios.	Indoor and outdoor IoT applications	A mathematical framework is provided and a MATLAB simulator is developed.	Performance evaluation is carried out in terms of PDR and energy consumption. The impact of parameters like end node density, virtual rings, deployment area coverage, area type, intermediate gateway density, and duty cycle are studied.	Do not consider downlink communications and retransmissions.
Related work					
[25]	Designed a LoRaWAN-compliant multi-hop uplink solution for existing gateways and evaluated the routing protocol's performance with a linear and bottleneck topology.	Outdoor IoT application	Not provided	PRR and throughput for a linear topology with a different number of end relay nodes	Did not study energy consumption, downlink communication, and retransmission.
[26]	Introduced epsilon multi-hop (EMH), a reinforcement learning (RL) technique based on epsilon-greedy, to enable reliable multi-hop typologies.	Indoor in an office building	Developed an RL algorithm to find energy-efficient routes.	Measured energy consumption to find the most energy-efficient routing and compared the results with single-hop.	Did not consider packet reception rate, downlink communications, and retransmission.
[27]	Implemented parallel SF transmission on a multi-hop network. Performance was significantly enhanced by using a tree-based SF clustering technique.	Outdoor IoT application	Provided a Tree-based SF clustering algorithm (TSCA).	Packet reception rate (PRR) and system air time depending on different SF allocation methods and different hop.	No consideration of intra-SF interference, not an efficient approach in terms of energy consumption.
[28]	Proposed a multiple-building area network using low-power nodes. Proposed sub-GHz LoRa as the physical-layer standard and a concurrent-transmission multi-hop network.	Multiple buildings	Equations to measure power margin and time delay for concurrent transmission.	Packet reception rate (PRR) depending on node number, hop number, and delay time.	No insight into relay node dependency on packet reception ratio and energy consumption.
[29]	Proposed an energy-efficient multi-hop communication solution (e2McH), which uses narrow-band technology.	All IoT applications	Offered an algorithm for E2MCH to optimize end-node energy usage.	Illustrated current consumption for both multi- and single-hop networks for a variety of LoRa bandwidths.	No insight into interference, retransmission, and acknowledgment.
[30]	Described a multi-hop LoRa approach to suggest an objective function for Low Power and Lossy Networks (RPL) facilitating selection of the ring-hop combination with the least air time.	Indoor and outdoor IoT applications	Equations for RPL to rank nodes in multi-hop network.	Ranks of the nodes in their multi-hop LoRa network.	No insight into the packet's successful ratio and energy consumption of the system.

connectivity with a low data rate and minimal power requirements. However, due to its similarities with the ALOHA protocol, which uses an unrestricted access method to a shared wireless frequency, LoRaWAN suffers from several drawbacks and limitations. Since a LoRaWAN end device may communicate data regardless of whether other end devices are busy or idle, packet collision can become a critical concern if many devices transmit signals at once. If numerous devices communicate with the gateway simultaneously, the average throughput might drop to less than 100 bits/s, especially for LoRa channels with high SF and the furthest nodes. Another contributing factor to the high packet collision rate in LoRaWAN is the lack of a defined channel evaluation method. Furthermore, according to the LoRa specifications [34], there can be only single-hop between the end devices and the gateway. In comparison with single-hop, multi-hop networks can enhance wireless network coverage and improve energy efficiency by using less transmission power. In addition, as mentioned in [35], multi-hop techniques may help increase scalability, capacity, and reliability. These multi-hop schemes also increase the technology's application reach, as it becomes a strong competitor in the IoT sector. Several researchers have proposed routing methods to allow multi-hop communication in LoRaWAN networks. After reviewing a number of different studies that are dedicated to evaluating the technology's potential as a multi-hop communication system, we categorized these articles into four distinct groups: experiment-based work, simulator-based work, analytical model-based work, and others. We present an orderly synopsis of these articles in Table 1 regarding research objectives, applications, studied parameters, and limitations.

The review reveals that comprehensive mathematical models dedicated to assessing corresponding multi-hop LoRaWAN have been almost unexplored in the literature. Moreover, in most cases, the approach devised in the literature is very specific as only a limited number of issues are addressed, making the analysis inconclusive and the extent of its application domain-bounded. Our work intends to address all the core issues and formulate relevant closed-form expressions to facilitate the systematic realization of the system modeled and lay out the platform to optimize and accommodate the key parameters.

III. SYSTEM DESCRIPTION

A. NETWORK TOPOLOGY

In this paper, class-A functionality and the ALOHA protocol are implemented on end devices for communication. Class A devices preserve duty cycle constraints by only using channels when they have packets to broadcast; otherwise, they are turned off. We suggest adopting inexpensive intermediate gateways instead of some end nodes (class-A) for packet forwarding [2]. For the intermediate gateway and end nodes, the SX1272 transceiver's capabilities are considered, while the SX1301 chip's capabilities are considered for the primary gateway connected to the Internet. To get packets from the
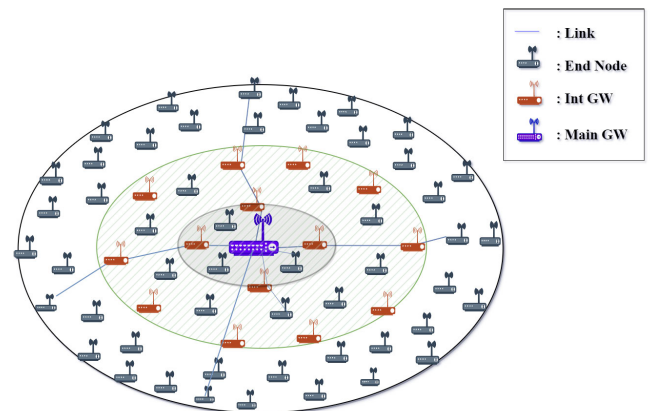

FIGURE 1. Multi-Hop LoRa-based network topology.

end nodes, eight of the chip's ten adjustable reception channels can be used. As a result, the device may simultaneously demodulate up to 8 packets [13].

The proposed approach is based on the extended-DRESG framework utilized in [36], where a tree network topology allows any kind of node positioning, and nodes are spread in distance-rings. As exhibited in Fig. 1, the protocol implements a multi-hop network structure based on LoRa. The end nodes are randomly deployed, and the main gateway is placed at the center. Utilizing a non-linear distance-spreading model, virtual rings are deployed around the main gateway in the system. The end nodes fall between two subsequent rings, and each network node is linked with its closest virtual ring. Afterwards, several clusters are devised in the system where a cluster defines a set of nodes having the same hop count to reach the main gateway. The cluster formation is contingent on the distance from nodes to the main gateway. The intermediate gateways are stationed in a suitable location of each ring (depending on the application scenario). In this paper, they are placed on the ring periphery.

The devices (end nodes or intermediate gateway) are employed with two options: they can send their packet directly to the main gateway if placed in any ring, or they can do so by using intermediate gateways close to the main gateway. However, the likelihood of each option occurring relies on the chosen routing strategy. In single-hop (SH) routing, the primary gateway and end nodes are in direct communication, whereas the device interfaces with the intermediate gateway of the immediate lower ring for the next-ring-hop (NRH) routing. Variable-hop (VH) routing is the name given to any other routing strategy that combines those two approaches.

The main gateway does not acknowledge packet receipt, and the devices do not retransmit packets. However, LoRaWAN permits up to eight re-transmissions, and it is the network designer's choice, along with the application's requirements, to determine how acknowledgment is used.

B. NETWORK ESTABLISHMENT

In the proposed communication system, a gateway forms a subset of the overall network, so it is necessary to assign

network addresses to each network produced by a gateway to facilitate network construction and multi-hop communication. Fig. 1 depicts a multi-hop communication arrangement with a main gateway and several intermediate gateways. We proposed utilizing LoRaWAN's standardized addressing technique described in the LoRaWAN specifications [10] with a few adjustments, which assigns a unique 3-byte network identity (ID) to each node in a LoRaWAN network. Also, LoRaWAN frames contain a "MessageType" field in the frame header that specifies the message type. The authors in paper [21] employed a similar approach. The routing protocol allows parallel collision-free transmission in this case. It considers that the main gateway has a list of all the device IDs (end node and intermediate gateways) and their locations associated with the ring position in the network. Likewise, the intermediate gateways and end nodes have a list of all the gateway IDs and information regarding their location and ring position.

1) INTERMEDIATE GATEWAYS NETWORK ESTABLISHMENT

The routing protocol defines two control messages: i) Intermediate Gateway Discovery (IG_DIS) and ii) Intermediate Gateway Response (IG_RES) [21]. The IG_DIS message consists of 10 bytes: message-ID (M_{ID}) - 1 byte, source ID (SG_{ID}) - 3 bytes, destination gateway ID (DG_{ID}) - 3 bytes, destination gateway ring ID (R_{ID}) - 1 byte, destination gateway hop count (H_{CNT}) - 1 byte and rebroadcast count (R_{CNT}) - 1 byte. Similarly, the IG_RES message is 7 bytes long: M_{ID} - 1 byte, SG_{ID} - 3 bytes and DG_{ID} - 3 bytes. The message formats for discovering and responding to intermediary gateways are depicted in Fig. 2a and 2b.

The main gateway initiates the process of building a network, finding intermediate gateways sequentially from the list provided, and creating forwarding pathways. First, the main gateway finds the intermediate gateways of the nearby ring; later, it can utilize them to find the intermediate gateways of the following rings. The main gateway broadcasts the IG_DIS message and sets the R_{CNT} field equal to R_{ID}. When any other intermediate gateway but the intended gateway receives the packet, it updates the SG_{ID} and reduces the R_{CNT} field by one before rebroadcasting the message. The IG_DIS message is not retransmitted if the R_{CNT} field is set to 0. When the targeted intermediate gateway receives the IG_DIS message, it stores the ring ID and the hop count. Afterward, it sends (back) an IG_RES message where the main gateway is set as the destination gateway. Then it stops acknowledging the IG_DIS message. Thus, the intermediate gateway connects with the nearest gateway of a particular ring or the main gateway as instructed in the H_{CNT}, allowing communications to proceed.

Once the main gateway receives the IG_RES message, it includes the ID of the intermediate gateway in its list of intermediate gateways which responded. The main gateway then starts searching for the next intermediate gateway in its list, which has yet to respond. This procedure is repeated until
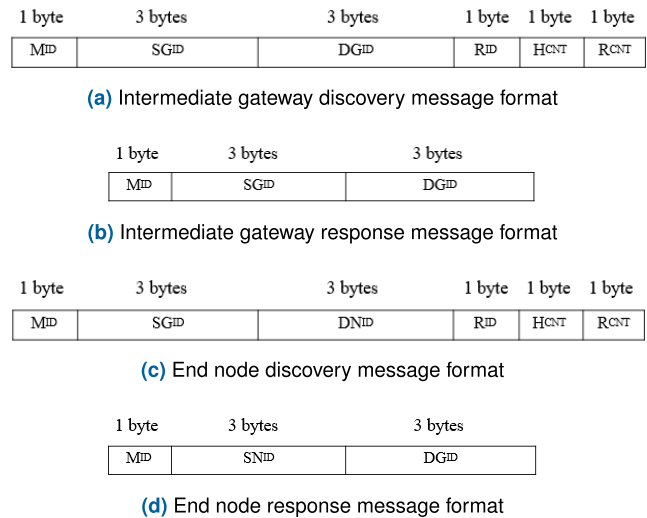

(a) Intermediate gateway discovery message format

(b) Intermediate gateway response message format

(c) End node discovery message format

(d) End node response message format

FIGURE 2. **Multi-hop communication protocol messages format.**

all intermediate gateways on the network have identified their respective forwarding gateways to the main gateway.

2) END NODES NETWORK ESTABLISHMENT

During this process, each node connects with only one intermediate gateway. The main gateway initiates this process, similar to the process described in the previous section. This protocol also employs two control messages: i) End node discovery (N_DIS), and ii) End node response (N_RES). The N_DIS message has a total size of 10 bytes: message-ID (M_{ID}) - 1 byte, source gateway ID (SG_{ID}) - 3 bytes, destination node ID (DN_{ID}) - 3 bytes, destination node ring ID - (R_{ID}) - 1 byte, destination node hop count (H_{CNT}) - 1 byte and rebroadcast count (R_{CNT}) - 1 byte. Similarly, the N_RES message is 7 bytes long: M_{ID} - 1 byte, source node ID (SN_{ID}) - 3 bytes and DG_{ID} - 3 bytes. The message formats for discovering an end node and its response are depicted in Fig. 2c and 2d, respectively.

The main gateway broadcasts a N_DIS message. When intermediate gateways receive this message, they reduce the R_{CNT} by 1 and update the S_{ID} with their ID before retransmitting the packet. The gateways will not broadcast the N_DIS message if the R_{CNT} field is set to 0. Ring ID and hop count are stored in the routing list when the end node receives the N_DIS message. Afterward, it transmits a N_RES message to the main gateway as a response. Upon receiving the N_DIS messages, the end node decides which parent is optimal, per the instruction in the H_{CNT}, favoring the one with the shortest distance.

C. COMMUNICATION MODEL

For the proposed system, we use the 868 MHz ISM band, which is the operating band for LoRa in Europe. According to the standard, it operates on two sub-bands, one at 868 MHz with three parallel sub-channels and the other at 867 MHz with five parallel sub-channels [37]. In our proposed system, downlink communications are not implemented. On the
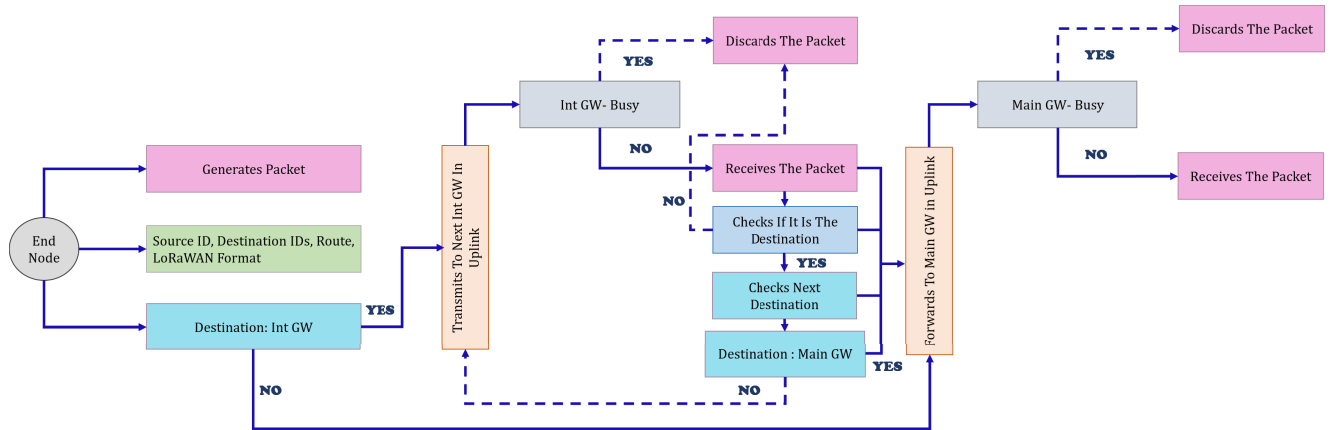
FIGURE 3. Communication model.

uplink, the end node and intermediate gateways arbitrarily select one sub-channel among the maximum six we consider for our system. The end nodes adhere to a duty cycle of 1 percent utilizing the ALOHA channel access mechanism [38]. The intermediate gateway continuously listens to these six channels when it is not transmitting [37]. LoRa offers six orthogonal spreading factors (SF7 to SF12), and we introduce a distance-based adaptive transmission configuration scheme in each device in the system to utilize one of them. Fig. 3 depicts the communication model considered for our system.

The packet format includes source node ID, destination node IDs, and hop counts. When the intermediate gateway picks a data packet at random from one of the six sub-channels, it checks if it is the destination. If not, it discards the packet. If it is, it forwards the data packet by using the reserved channel to the intermediate gateway in the upper ring or the main gateway, according to the routing scheme utilized. Note that the intermediate gateway will not generate a packet on its own. Any other data packet arriving will be discarded when the intermediate gateway is in the transmitting phase. The approach adopted in this work, unlike the original model [39], considers that the intermediate gateway forwards a data packet without any delay upon its successful reception. Therefore, additional delays are not included in the study. The main gateway always monitors the available uplink channels and forwards any received packet to the network server. However, when the main gateway is busy receiving a transmission on a particular channel, another packet arriving on the same channel is not decoded.

IV. MATHEMATICAL MODELING OF MULTI-HOP LoRa NETWORK

A. ASSUMPTIONS

We make a number of assumptions in the establishment of our model. First, all nodes and gateways are location and distance aware, minimally of their location and their intended receivers (intermediate gateways or the main gateway). Second, the deployment of the nodes is made on a disc, which can be decomposed into rings.

B. RING PLACEMENT

In the DRESG framework, rings are placed using one of the following selected distance spreading models: Equidistant, Fibonacci, or Reverse Fibonacci (R-Fibonacci) [23]. The last ring is positioned at the deployment area radius, denoted by L. The equidistant spreading model positions the distance of any ring m proportionally to the total number of rings M, i.e., $l_{\text{equi}}(m) = m(L/M)$. Conversely, the Fibonacci spreading model positions the rings so that the distance between rings increases as the rings are further away from the gateway. The R-Fibonacci model sets the distance between rings in decreasing order. The Fibonacci model, adopted in our analysis to set inter-ring distance, is expressed using the following expression: [23],

$$l_{\text{fibo}}(m) = \frac{F_{m+1}L}{F_{M+1}} \qquad (1)$$

where F_n is the nth number of Fibonacci sequence.

C. DETERMINATION OF CHILD-PARENT RELATIONSHIP

A crucial concern in the multi-hop network is determining the packet forwarding route. For a system constructed with N_e end nodes, the ring-hop combination is denoted as P, and P_i refers to the hop count for the nodes in a ring i, and the number of nodes in a ring i is denoted as N_{ei} where $i \in [1, M]$. The number of nodes under an intermediate gateway of a ring i is expressed by $CN_i = TH$ where TH is the maximum number of nodes that are set to be supported by an intermediate gateway in the system. To be specific, consider an example with M = 4 and a defined ring-hop combination of $P = [1, 1, 1, 3]$, where $P_1 = 1$ denotes that nodes of ring 1 forward packets to the main gateway while nodes of ring 2 transmit packets to IGs set at ring 1. In the same manner, nodes of ring 3 send packets to IGs positioned at ring 2. The nodes placed in ring 4 transmit their packets to IGs positioned at ring 1.

A child-parent relationship matrix, R, is developed to find out the relationship between two rings in the system according to any routing scheme using the following

condition:

$$r_{ij} = \begin{cases} 1 & i < j \ \& \ i = j - P_j \\ 0 & \text{otherwise} \end{cases} \quad (2)$$

R is a $M \times M$ (0, 1)-matrix. The (i, j) element, denoted by r_{ij}, indicates whether a child-parent relationship exists according to the defined ring-hop combination between two rings or not. If $r_{ij} = 1$, then it indicates that the j_{th} ring forwards its data to the i_{th} ring. The connectivity matrix is defined as:

$$R = \begin{bmatrix} 0 & 1 & 0 & \cdots & 0 \\ 0 & 0 & 1 & \ldots & 0 \\ 0 & 0 & 0 & \cdots & 1 \\ \vdots & \vdots & \vdots & \vdots & \vdots \\ 0 & 0 & 0 & \cdots & 0 \end{bmatrix}$$

D. NUMBER OF INTERMEDIATE GATEWAYS

Depending on the routing mechanism, the end nodes in a multi-hop network forward data packets to intermediate gateways or the main gateway. Therefore, determining the number of intermediate gateways in the system is crucial. To facilitate the expression of the dynamic allocation of intermediate gateways in the system, we introduce the following symbols.

$$ig_{oi} = \left\lceil \left(\sum_{j=1}^{M} \left(r_{ij} \times \frac{N_{ej}}{CN_j} \right) \right) \right\rceil \quad (3)$$

ig_{oi} is the number of required intermediate gateways in a ring i to relay the data from the end nodes of the upper ring.

$$ig_i = \left\lceil \left(\sum_{j=1}^{M} \left(r_{ij} \times \frac{(N_{ej} + ig_{oi})}{CN_j} \right) \right) \right\rceil \quad (4)$$

ig_i is the number of required intermediate gateways in a ring i to support the intermediate gateways and nodes of the upper ring.

Throughout the paper, we use N_{ig} to represent the total number of intermediate gateways while N is the total number of devices (end nodes and intermediate gateways) in the system.

E. HOP DEPENDENT TRANSMISSION RANGE ESTIMATION MODEL

A device adjusts its transmission power and current such that its packets reach their intended receiver (gateway) while avoiding unnecessary power consumption. First, the distances between an upper ring end node and the accessible lower ring intermediate gateways are calculated, and then the closest receiver is sorted out.

In our system, T is a $N_e \times N_{ig}$ euclidean distance matrix where element t_{uv} describes the distance between a node u from ring j and an intermediate gateway v from ring i, if nodes of the ring j forward their data to intermediate gateways of

ring i. The matrix element t_{uv} is computed using the following expression:

$$t_{uv} = r_{ij} \times d_{uv} \quad (5)$$

where d_{uv} is the euclidean distance between the node u and intermediate gateway v, where $u \in \left[u'_{j-1} + 1, u'_{j-1} + N_{ej} \right]$ and $v \in \left[v'_i + 1, v'_i + ig_i \right]$.

The expression u' is used to identify the nodes of the one ring that can establish a link with the intermediate gateways of another particular ring, and the expression v' is used to determine those intermediate gateways if the two rings are associated with each other according to r_{ij}. The following expressions are developed to compute the values of u' and v':

$$u'_{j-1} = \sum_{m=1}^{j-1} \left(u'_m + N_{em} \right) \quad (6)$$

$$v'_i = \sum_{k=2}^{i} \left(v'_k + ig_{k-1} \right) \quad (7)$$

where $j \in [1, M]$ and $i \in [1, M]$.

Another $N_{ig} \times N_{ig}$ euclidean distance matrix W is developed where element w_{pq} describes the distance between intermediate gateway p from ring i and q from ring j if intermediate gateways of the ring j forward their data to intermediate gateways of ring i. The matrix element w_{pq} is computed using the following expression:

$$w_{pq} = r_{ij} \times d_{pq} \quad (8)$$

where d_{pq} is the euclidean distance between the intermediate gateway p and intermediate gateway q, where $p \in \left[p'_{j-1} + 1, p'_{j-1} + ig_j \right]$ and $q \in \left[q'_i + 1, q'_i + ig_i \right]$. The term p' is employed in specifying intermediate gateways of the one ring that can set up a link with the intermediate gateways of another particular ring, which are addressed by utilizing q' if a relationship exists between the two rings as determined by r_{ij}. The following expressions are developed to compute the values of p' and q':

$$p'_{j-1} = \sum_{m=1}^{j-1} \left(p'_m + ig_m \right) \quad (9)$$

$$q'_i = \sum_{k=2}^{i} \left(q'_k + ig_{k-1} \right) \quad (10)$$

where $j \in [1, M - 1]$ and $i \in [1, M - 1]$.

Then, the N euclidean distance vector DM is formulated where element dm_i denotes the distance between a device i and the main gateway. To define the estimated transmission range of each device in the system, a vector D is formulated where component d_i describes the distance between a device i and its destination. The component d_i is computed based on

the following expressions:

$$
d_i = \begin{cases}
\min\left(t_{jk}\right), & \sum_{k=1}^{N_{ig}} t_{jk} > 0, j = i, \\
i \in [1, N_e] & \\
\min\left(w_{jk}\right), & \sum_{k=1}^{N_{ig}} w_{jk} > 0, j = i - N_e, \\
i \in \left[1 + N_e, N_e + N_{ig}\right] & \\
dm_{1i} &
\end{cases}
\tag{11}
$$

F. APPLICATION MODEL

Devices are modeled to generate traffic randomly. After transmitting the first packet randomly in a user-defined range, the device waits for T_{off} seconds to transmit its next data packet while respecting the duty cycle limitations, D_c. T_{off} is defined by the following expression [40],

$$
T_{\text{off}} = \text{ToA} \times (100 - D_c) + \Delta_t
\tag{12}
$$

where Δ_t is the random delay parameter and ToA is Time-on-Air defined as [31],

$$
\begin{aligned}
\text{ToA} = \frac{2^{\text{SF}}}{\text{BW}} * \Bigg(& \left(n_{\text{preamble}} + 4.25\right) + 8 \\
& + \max\left(\left\lceil\left(\frac{8PL - 4SF + 28 + 16 - 20H}{4(SF - 2DE)}\right)\right\rceil\right. \\
& \left.\times (CR + 4), 0\right)\Bigg)
\end{aligned}
\tag{13}
$$

where $n_{preamble}$ denotes preamble size, PL is payload size, H defines header mode, which is set to 1 or 0 to indicate implicit or explicit header, and DE is set to 0 or 1 to enable or disable low data rate optimization. Here, BW denotes bandwidth, SF is the spreading factor, and CR is the coding rate ranging from 1 to 4.

G. PERFORMANCE EVALUATION MODEL

1) PATH LOSS MODEL

For a successful packet reception, the received signal power P_{rx} ought to be greater than the receiver's sensitivity threshold S_{rx}. Transmit power P_{tx} and all gains and losses along the communication path [32] determine the received power:

$$
P_{rx} = P_{tx} + GL - L_{pl}
\tag{14}
$$

P_{rx} denotes the received power in decibels, P_{tx} is the transmitted power in decibels, GL is the sum of all general gains, such as transmitter antenna gain and receiver antenna gain, and losses, such as transmitter loss and receiver loss, while L_{pl} denotes the path loss, which is based on the characteristics of the environment in which the system is deployed. Initially, we have considered 4 different cases regarding system environments to characterize their impacts on the system's performance. The analysis includes urban, suburban, and rural

TABLE 2. Transceiver's output power P_{tx} and current consumption I_{tx} [14].

Model	Setting	P_{tx}(dBm)	I_{tx}(mA)	I_{rx}(mA)
SX1272	1	20	125	10.5
	2	17	90	
	3	13	28	
	4	7	18	

settings as well as an outdoor scenario considering pico/hot zone deployment.

We used the path loss model for 802.11ah to accurately model the wireless channel in the outdoor environment. This channel model provides a realistic representation of the characteristics of signal propagation in outdoor environments, making it well-suited for our study. Studies similar to our approach, such as [23] and [36], have also employed the 802.11ah channel model to investigate the performance of wireless networks in outdoor environments. For the open-space scenario, L_{pl} is calculated utilizing the outdoor path loss model for 802.11ah pico/hot zone deployments adopted from [41],

$$
L_{pl(outdoor)} = 23.3 + 37.6 \log_{10}(d) + 21 \log_{10}\left(\frac{f}{900\text{MHz}}\right)
\tag{15}
$$

where f is the frequency in MHz and d is the distance in meters between transmitter and receiver. For an urban scenario, the Okumura–Hata model is utilized to calculate L_{pl} [42],

$$
\begin{aligned}
L_{pl(urban)} = {} & 69.55 + 26.16 \log_{10}(f) - 13.82 \log_{10}\left(h_r\right) - c_h \\
& + \left(44.9 - 6.55 \log_{10}\left(h_r\right)\right) \cdot \log_{10}(\frac{d}{1000})
\end{aligned}
\tag{16}
$$

For a suburban scenario, L_{pl} is calculated utilizing Okumura–Hata model [42],

$$
L_{pl(suburban)} = L_{pl(urban)} - 2\left(\log_{10}\frac{f}{20}\right)^2 - 5.4
\tag{17}
$$

For a rural scenario, L_{pl} is calculated utilizing Okumura–Hata model [42],

$$
\begin{aligned}
L_{pl(rural)} = {} & L_{pl(suburban)} - 4.78\left(\log_{10}f\right)^2 \\
& + 18.33 \log_{10}f - 40.97
\end{aligned}
\tag{18}
$$

where h_r is the receiver antenna height (m) and ch is the antenna height adjustment factor, which depends on the frequency and the extent of the area concerned and is specified by the following,

$$
c_h = 0.8 + \left(1.11 \log_{10}f - 0.7\right)h_t - 1.56 \log_{10}f
\tag{19}
$$

where h_t is the transmitter antenna height (m). Expression (19) applies to medium and small-size areas. The transceiver selects the optimum transmission configurations from Table 2 accordingly to cover the distance d. Table 2 summarizes the relevant power and current consumption specifications of the SX1272 transceiver [14].

SF	7	8	9	10	11	12
SNR[dB]	-7.5	-10	-12.5	-15	-17.5	-20

2) RECEIVER SENSITIVITY

The sensitivity of a radio receiver at room temperature is computed using the following expression adopted from [11],

$$S_{rx} = -174 + 10 \log_{10}(BW + NF + SNR) \quad (20)$$

The receiver's temperature is the primary factor that may affect the first term, which defines thermal noise in a 1 Hz bandwidth. NF denotes the constant receiver noise figure, and SNR is the signal-to-noise ratio determined by the spreading factor (Table 3).

3) INTERFERENCE

It is assumed that the interference can only originate from other LoRa signals to evaluate how the LoRaWAN network will behave in the multi-hop configuration. Therefore, a number of factors, including timing, transmission region, carrier frequency (CF), spreading factor (SF), and power, must be considered to analyze the interference in the multi-hop LoRa network.

- **Reception Overlap:** For a packet i, a reception interval $\in (T_{bi}, T_{ei})$ denotes that T_{bi} marks the beginning of packet reception while $T_{ei} = T_{bi} + ToA_i$ defines the end of reception. The midpoint is defined by $m_i = (T_{bi} + T_{ei})/2$ and the midpoint length by $h_i = (T_{bi} - T_{ei})/2$. To determine the reception intervals overlap of two packets, i and j, the following expression is exploited [32]:

$$O(i, j) = |m_i - m_j| < h_i + h_j \quad (21)$$

- **Transmission Region:**
  To describe the event of whether two devices are utilizing the same transceiver (intermediate gateway or main gateway) as the receiver, a $N \times N$ (0, 1) - connectivity matrix A is constructed. Note that the mathematical framework described in section IV-E is utilized to devise the matrix. The matrix's (i, j) element is represented by the a_{ij}, where $a_{ij} = 1$ refers to the same receiver utilization by device i and device j and $a_{ij} = 0$ refers to different receiver utilization. The matrix elements are updated in each corresponding hop as the different devices can utilize different gateways (intermediate or main) in their corresponding hops. The matrix is defined as follows:

$$A = \begin{bmatrix} 0 & 1 & 0 & \dots & 1 \\ 1 & 0 & 1 & \dots & 0 \\ 0 & 1 & 0 & \dots & 1 \\ \vdots & \vdots & \vdots & \vdots & \vdots \\ 1 & 0 & 1 & \dots & 0 \end{bmatrix}$$

- **Intra-SF Interference and Intra-Channel Interference:**
  The list of SFs utilized by the N devices in the system is described by the set $\mathbf{SF_{all}} = \{SF_1, \dots, SF_N\}$. Similarly, $\mathbf{CH_{all}} = \{CH_1, \dots, CH_N\}$ represents the set of channels utilized by the N devices. Note that the value of the sets is updated depending on the selected transmission parameter.
  A connectivity matrix S, which is a $N \times N$ (0, 1) - matrix, is devised to describe the occurrence when the SF of one device matches that of another. The matrix's (i, j) element is represented by the s_{ij}, where $s_{ij} = 1$ denotes a match between SF_i and SF_j and $s_{ij} = 0$ denotes a mismatch. Similarly, the matrix Z specifies what happens when two devices use the same channel, where the (i, j) element is represented by the z_{ij}. Below are two potential values for the matrices S and Z [43].

$$S = \begin{bmatrix} 0 & 1 & 0 & \cdots & 1 \\ 1 & 0 & 1 & \cdots & 0 \\ 0 & 1 & 0 & \cdots & 1 \\ \vdots & \vdots & \vdots & \vdots & \vdots \\ 1 & 0 & 1 & \cdots & 0 \end{bmatrix} \quad Z = \begin{bmatrix} 0 & 1 & 0 & \cdots & 1 \\ 1 & 0 & 1 & \cdots & 0 \\ 0 & 1 & 0 & \cdots & 1 \\ \vdots & \vdots & \vdots & \vdots & \vdots \\ 1 & 0 & 1 & \cdots & 0 \end{bmatrix}$$

- **Power:**
  When more than one packet is present at the receiver, the interference condition based on power occurs. The capture effect can affect LoRa networks. The stronger signal suppresses the weaker signal when two signals are present at the receiver, which is known as the capture effect. As a result, the received signal intensities could not vary significantly whenever the difference falls below a predetermined threshold and is too small. However, the receiver repeatedly switches between the two signals, making it impossible to decode either transmission [32]. Thus, inter-SF interference is evaluated. The following equation describes this phenomenon [44]:

$$(P_{rxi} - P_{rxj}) < P_{\text{th}} \quad (22)$$

where P_{rxi} is the receiving end power for the desired packet transmitted by node i and P_{rxj} is the receiving power of the interfering packet sent by node j. P_{th} is the corresponding SINR (signal-to-interference-plus-noise-ratio) power in dB above which the received power difference needs to be decoded by the receiver, described by the Table 4 [44]. Based on the condition described by expression (22), a connectivity matrix Ξ is defined, which is a $N \times N$ (0, 1) - matrix, where (i, j) element of the matrix is denoted by ξ_{ij}.

$$\Xi = \begin{bmatrix} 0 & 0 & 1 & \dots & 1 \\ 0 & 0 & 1 & \dots & 0 \\ 1 & 1 & 0 & \dots & 0 \\ \vdots & \vdots & \vdots & \vdots & \vdots \\ 1 & 0 & 0 & \dots & 0 \end{bmatrix}$$

TABLE 4. SINR thresholds (dB).

Interferer Desired	SF-7	SF-8	SF-9	SF-10	SF-11	SF-12
SF-7	6	-16	-18	-19	-19	-20
SF-8	-24	6	-20	-22	-22	-22
SF-9	-27	-27	6	-23	-25	-25
SF-10	-30	-30	-30	6	-26	-28
SF-11	-33	-33	-33	-33	6	-29
SF-12	-36	-36	-36	-36	-36	6

- **Interference Conditions:**

Case I: Packets transmitted by the end nodes can interfere on multiple occasions. The first scenario is when two nodes share a gateway and the gateway simultaneously takes in transmitted packets. No packet is decoded by the receiver when two packets i and j overlap in their reception at the same receiver with the same SF, same channel [32], [45], and the difference of their signal strengths is lower than the cutoff set by Table 4. This can be described by $a_{ij} \wedge s_{ij} \wedge z_{ij} \wedge \xi_{ij} = 1$, which means that neither packet i nor j is received if they overlap in their reception.

Case II: Packets can collide even with different spreading factors if they overlap at reception and the following circumstance holds true: $a_{ij} \wedge z_{ij} \wedge \xi_{ij} = 1$.

Case III: A LoRa transmission is received if $P_{rx} > S_{rx}$ [32], [45]. Exploiting expression (14), (15), and (20), it can be determined whether a transmission will be decoded or not.

Based on the three cases discussed, we develop a $N \times N(0, 1)$ connectivity matrix C. The (i, j) element of the matrix is denoted by c_{ij}, where $c_{ij} = 1$ refers to the potential interference event of i_{th} node with the j_{th} node while $c_{ij} = 0$ refers to no interference between the two nodes. Note that, $c_{ii} = 1$ refers that $P_{rxi} < S_{rxi}$. The matrix is described as follows, and it might change values depending on the context:

$$C = \begin{bmatrix} 1 & 0 & 1 & \cdots & 1 \\ 0 & 0 & 1 & \dots & 0 \\ 1 & 1 & 1 & \cdots & 1 \\ \vdots & \vdots & \vdots & \vdots & \vdots \\ 1 & 0 & 1 & \cdots & 0 \end{bmatrix}$$

Using this matrix, we derive a diagonal $N \times N(0, 1)$ matrix U to describe the state of a data packet. The diagonal elements u_{ii} are set to 0 or 1 based on the following condition:

$$u_{ii} = \begin{cases} 1, & \sum_{j=1}^{N} c_{ij} > 0 \\ 0, & \text{otherwise} \end{cases} \quad (23)$$

Then the total number of packets lost in the system is calculated using the following expression:

$$N_c = \int_{T_i}^{T_e} \left(\sum_{i=1}^{N} u_{ii} \right) dt \quad (24)$$

where N_c denotes the number of packets lost in the network observation period. Observation starts at T_i and ends at T_e.

The packet delivery ratio is calculated using the following expression:

$$P_{dr} = (N_s - N_c) / N_s \quad (25)$$

where N_s is the number of the total sent packets in the system during the whole network operation time.

- **Energy Consumption:** The transmission energy consumed by the node or intermediate gateway can be calculated using the following expression [23]:

$$e_{tx} = ToA_{tx} \times I_{tx} \times V_{op} \quad (26)$$

where e_{tx} is the transmission energy consumed by the device (end node or IG) during a transmission, ToA_{tx} is Time-on-Air of the transmitted packet, and I_{tx} is transmission current according to the settings exploited by the transceiver and V_{op} is the operating voltage of the transceiver.

The energy consumed by an intermediate gateway during the reception of a packet is calculated using the following expression [23]:

$$e_{rx} = ToA_{rx} \times I_{rx} \times V_{op} \quad (27)$$

where e_{rx} is the energy consumed by the intermediate gateway during a reception, ToA_{rx} is Time-on-Air of the received packet, and I_{rx} is RX current consumption [23]. The total energy consumption of the network system is:

$$E_{\text{total}} = \sum_{i=1}^{N_s} e_{tx\,i} + \sum_{j=1}^{N_{sig}} e_{tx\,j} + \sum_{k=1}^{Nrig} e_{rx\,k} \quad (28)$$

where $Nsig$ is the number of total packets forwarded by the intermediate gateways and $Nrig$ is the number of total packets received by the intermediate gateways in the observation duration.

V. EVALUATION FRAMEWORK

For any combination of network design parameters, such as the number of virtual rings, ring positions, or intermediate gateway deployment, the framework in Fig. 4 can be utilized as a tool by network designers to assess the performance of various routing processes and various setups. This framework was built on the analysis in the previous section.

The deployment of the nodes and gathering data on node positions make up the first stage. In this research, end nodes are uniformly distributed. The rings are positioned using the Fibonacci distance-spreading-model in this paper. Algorithm 1 shows the connectivity establishment procedure. A ring-hop combination adaptive intermediate gateway allocation scheme is then used to determine the required number of intermediate gateways. Transmission parameters like
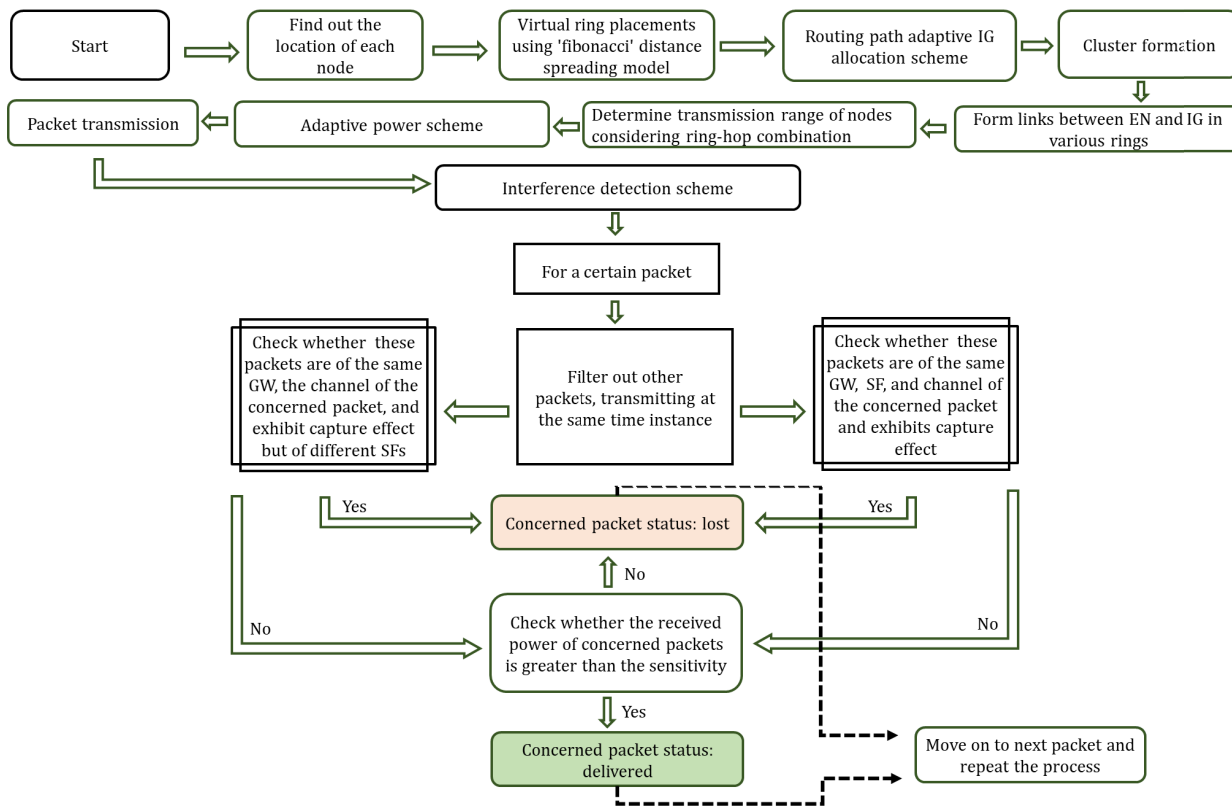
FIGURE 4. Evaluation framework.

Algorithm 1 Connectivity Establishment

Data: ring-hop combination P, Number of rings M
Result: Connectivity between rings

1 **Initialization**
2 $r_{ij} \leftarrow 0$;
3 **for** $1 \leq i \leq M$ **do**
4   **for** $1 \leq j \leq M$ **do**
5   **if** $i \leq j$ *AND* $i == j - P(j)$ **then**
6          $r_{ij} \leftarrow 1$;   /* ring j forwards data to ring i */
7   **end**
8   **end**
9 **end**
10 **return** Connectivity between rings

---

transmission power, current and spreading factor are set utilizing a distance-based scheme in which every network module chooses the transmission configuration according to its distance from the targeted receiver, described in Algorithm 2. This scheme aims to keep the system's energy usage to a minimum.

To guarantee that the network's connectivity is functional, we built a packet reception check mechanism to make it easier to determine whether a packet reaches the receiver end. Several filtering mechanisms are devised as discussed in the

---

Algorithm 2 Computation of Distance-Based Adaptive Transmission Parameters

---
Data: Transceiver's available setting list=se, transmit power list=P_{se}, current list=I_{se}
Data: User defined spreading factors list=SF_{se}, transceiver's estimated coverage list=d_{se} - for corresponding setting
Data: Transceiver's targeted coverage=d, maximum coverage=D_{max}, setting =st, transmit power=P_{tx}, transmit current=I_{tx}, spreading factor=SF
Result: P_{tx}, I_{tx}, SF

1 **for** $1 \leq j \leq length(se)$ **do**
2   **if** $d \leq d_{se}(j)$ **then**
3       $st \leftarrow j$ terminate the loop;
4   **else if** $d > D_{max}$ **then**
5       $st \leftarrow length(se)$;
6   terminate the loop;
7 **end**
8 $P_{tx} = P_{se}(st)$;
9 $I_{tx} = I_{se}(st)$;
10 $SF = SF_{se}(st)$;
11 **return** P_{tx}, I_{tx} and SF

---

previous section IV-G and are illustrated in the Algorithm 3. The data from the transceiver and path-loss model are then

Algorithm 3 Packet Reception

Data: Desired packet d, Interferer i, Corresponding hop h
Data: SF - spreading factor of packet
Data: CH - channel utilized by packet
Data: Route data - GWs utilized by the desired packet
Data: P_ rx - power of the packet (transmitted by node)
Data: P_rxg power of the packet (transmitted by IG)
Data: Duration - in which packet might be available
Result: receiving status = 0 if packet lost or receiving status = 1 if delivered

1 **Initialization**
2 receiving status of the packet = 1;
3 **for** _interferer ∈_
  packets that are available in the duration of desired packet
  do
4 | **if** _interferer's GW = packet's GW AND interferer's SF = packet's SF AND interferer's CH = packet's CH AND_ $P_{rxdh} - P_{rxih} < P_{th}$ **then**
5 | | receiving status of the packet = 0;
6 | | terminate the loop;
7 | **end**
8 | **if** $P_{rxdh} < S_{rxdh}$ **then**
9 | | receiving status of the packet = 0;
10 | | terminate the loop;
11 | **end** **if** _desired packet is forwarded by IG_ **then**
12 | | **for** _interferer ∈_
    | | _packets that are forwarded by IG_ **do**
13 | | | **if** _interferer's GW = packet's GW AND interferer's SF = packet's SF AND interferer's CH = packet's CH AND_ $P_{rxgdh} - P_{rxgih} < P_{th}$ **then**
14 | | | | receiving status of the packet = 0;
15 | | | | terminate the loop;
16 | | | **end**
17 | | **end**
18 | | **if** $P_{rxgdh} < S_{rxgdh}$ **then**
19 | | | receiving status of the packet = 0;
20 | | | terminate the loop;
21 | | **end**
22 | **end**
23 **end**
24 **return** receiving status of the packet;

used to compute the energy consumption of the network system during packet transmission and reception.

VI. SIMULATION RESULTS

Simulations were carried out in MATLAB. The parameters adopted to simulate the multi-hop LoRa network for different configurations considered in our simulations is summarized

TABLE 5. Simulation parameters.

No. of nodes	50 to 500	Cell radius	3 to 11 [km]
Node distribution	Uniform	Duty cycle	1 %
No. of rings	1 to 3	Gain	0 B
No. of channels	6	Bandwidth	125 kHz
Preamble length	8 bytes	Scenario	Outdoor
Payload length	20 bytes	Simulation length	600 seconds
Operating voltage of module	3 V	Transmit power	[7,13,17,20] dB
Coding rate	1	Transmit current	[18,28,90,125] mA
Transmitter antenna height	1 m	Receiver antenna height	24 m
Δ_t	[1,20] seconds	Battery capacity	[1000] mAh
Spreading factors	7 to 12	Reception current	10.5 mA

TABLE 6. Choice of transmission configurations based on distance-based adaptive transmission parameter selection scheme.

Distances (m)	P_{tx} (dBm)	SF	I_{tx} (mA)	Energy Consumption (mJ)
770	7	[7 8 9 10 11 12]	18	[2.7 5 10 17.8 35.6 62.3]
	13	[7 8 9 10 11 12]	28	[4.3 7.7 15.5 27.6 55.3 97]
	17	[7 8 9 10 11 12]	90	[13.8 25 50 89 178 311.8]
	20	[7 8 9 10 11 12]	125	[19.2 34.7 69.5 123.6 247.3 433.1]
2000	13	[11 12]	28	[55.3 97]
	17	[10 11 12]	90	[89 178 311.8]
	20	[9 10 11 12]	125	[69.5 123.6 247.3 433.15]
3100	20	[11 12]	125	[247.3 433.15]

in Table 5. The key aspects evaluated are discussed in the subsequent sections.

A. EVALUATION OF THE DISTANCE-BASED ADAPTIVE TRANSMISSION PARAMETER SELECTION SCHEME

Table 6 presents the available options for transmission configurations and the transmitter's corresponding energy consumption for transmitting a data packet to a specific distance. The proposed algorithm allows for selecting the transmission configuration that results in minimum energy expenditure from the available options. To illustrate the algorithm's effectiveness, consider the first example case presented in Table 6. In this case, several options are available for transmitting data over a distance of 770 meters. The proposed algorithm selects the configuration[1] with $P_{tx} = 7$ dBm, $SF = 7$, and $I_{tx} = 18$ mA, leading to a minimal energy consumption of 2.77 mJ for this case. This example highlights the ability of

[1]Selected parameters are highlighted with red color.

TABLE 7. Impact of path loss model selection.

Type	Model	Maximum Coverage (km)	Cases	Distance (km)	Path Loss (dB)
Outdoor	802.11ah	3.67	1	0.77	131.5
			2	2	147.09
Urban	Okumura-Hata	6.2	1	0.77	124.53
			2	2	139.39
Suburban	Okumura-Hata	11.682	1	0.77	113.77
			2	2	128.63
Rural	Okumura-Hata	38.327	1	0.77	84.414
			2	2	99.279
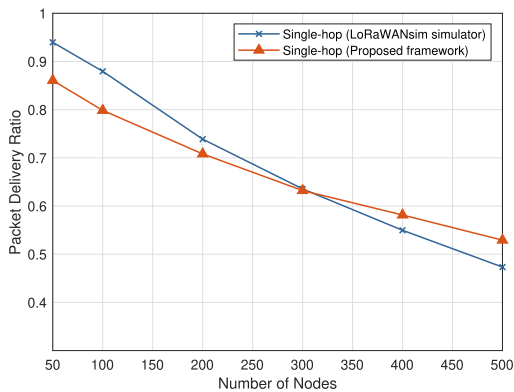
FIGURE 5. Protocol validation in terms of PDR.

FIGURE 6. Protocol validation in terms of energy consumption.

FIGURE 7. Comparison of PDR for multi-hop and single-hop LoRa networks in sparse and dense deployments.

FIGURE 8. Comparison of energy consumption for multi-hop and single-hop LoRa networks in sparse and dense deployments.

the proposed algorithm to efficiently optimize the energy consumption of LoRa devices, even in scenarios where multiple transmission options are available.

B. COVERAGE RADIUS IN DIFFERENT ENVIRONMENT SCENARIOS

The maximum coverage radius for devices deployed in the network is analyzed for various environmental conditions using the associated path loss models, as shown in Table 7 and utilizing information about the SX1272 transceiver from [14]. The coverage is found to be maximum (of 38.327 km) in the rural environment due to lower attenuation and 3.67 km in the outdoor environment due to high attenuation [36]. The path loss varies from one environment to another for a specific distance. The outdoor path loss model for 802.11ah pico/hot zone is employed for the rest of the simulations.

C. RELIABILITY OF THE PROPOSED FRAMEWORK

We employed the LoRaWANSim simulator developed by [46] and widely used in similar studies related to LoRaWAN to validate our proposed framework. We compared the data obtained from our proposed framework with the data extracted from the simulator. The evaluation is restricted to the single-hop (SH) implementation since the reference simulator does not employ multi-hop communication. We obtained data for packet delivery ratio and energy consumption per packet transmission, which were found to be close to the data retrieved from the reference simulator, thus setting a reference baseline. This similarity between the
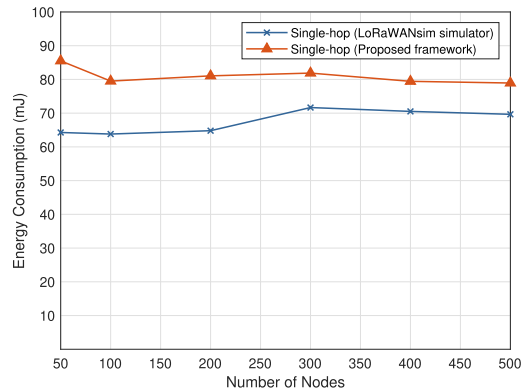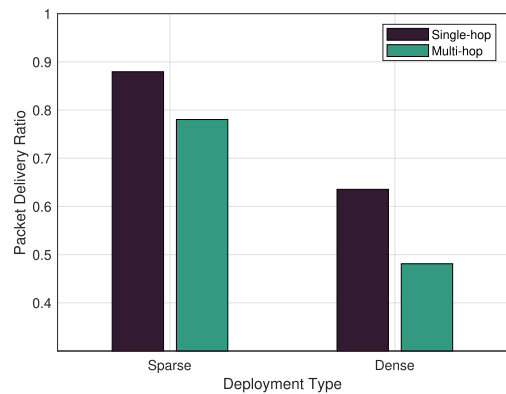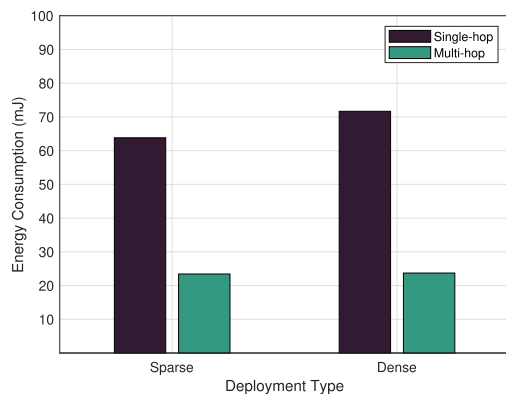
two sets of data reflects the soundness of our framework in accurately representing the performance of single-hop LoRaWAN. The simulation parameters were the same for the results presented in Fig. 5 and Fig. 6. Nonetheless, there were certain inherent differences between the simulator considered and our proposed framework. In this case, the deployment region was set to 3 km.

D. PERFORMANCE EVALUATION IN SPARSE AND DENSE DEPLOYMENTS

To evaluate the performance of the proposed framework in both sparse and dense cases, we conducted an analysis
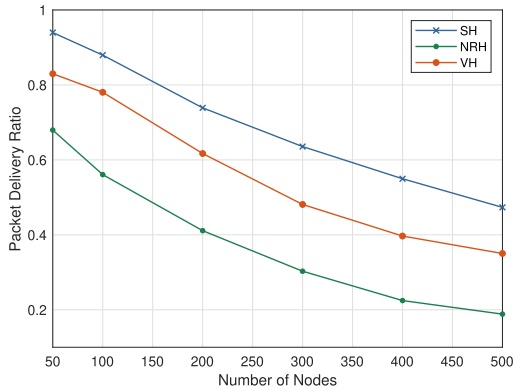
FIGURE 9. Impact of Node Density: $A_r = 3$ km, $TH = 6$, $\Delta_t = [1, 20]$.

FIGURE 10. Impact of deployment area Radius on PDR: $N_e = 100$, $TH = 6$, $\Delta_t = [1, 20]$.

FIGURE 11. Impact of deployment area Radius on end node's energy consumption: $N_e = 100$, $TH = 6$, $\Delta_t = [1, 20]$.

considering a deployment region radius of 3 km with 100 nodes for sparse deployment and 300 nodes for dense deployment scenarios. We considered $TH = 6$, $\Delta_t = [1, 20]$, and 3 virtual rings for the multi-hop cases. Our findings, depicted in Fig. 8, demonstrate that multi-hop outperforms single-hop for sparse and dense deployment scenarios in the case of energy savings. The energy consumption per packet transmission is reduced by 60% in sparse deployment and 70% in dense deployment, indicating the potential benefits of multi-hop routing in both scenarios. However, single-hop LoRaWAN performs better in delivering packets for the considered cases shown in Fig. 7 since it avoids packet loss due to relaying and utilizes the LoRa node's maximum coverage of up to 3.67 km.

E. IMPACT OF NODE DENSITY
In Fig. 9, the impact of node density on the performance of the proposed multi-hop LoraWAN is evaluated in comparison to the standard single-hop LoRaWAN for $A_r = 3$ km, $TH = 6$, $\Delta_t = [1, 20]$ and 3 virtual rings. As node density increases, the PDR drops due to the increasing number of packets in the system leading to more frequent collisions. The result reveals that for dense deployment and areas less than 3.67 km, single-hop LoRaWAN outperforms multi-hop LoRaWAN by providing about 10% more PDR than VH routing. In this case, NRH routing performs the worst because the frequency of packet relaying is highest for NRH.

F. IMPACT OF DEPLOYMENT AREA RADIUS
For a system with 100 nodes, $TH = 6$, $\Delta_t = [1, 20]$, and 3 virtual rings, it is observed that the performance of single-hop LoRaWAN degrades as the deployment area radius is extended (Fig. 10). The probability of packet loss due to increased interference with more packet relays. However, for the considered scenario, NRH routing still has the lowest PDR. For area radii up to 3.67 km, SH routing performs the best. The primary issue, despite interference issues in the system, that is contributing to the sharp performance loss is that as the region radius exceeds 3.67 km, an increasing number of nodes become unable to connect to the main gateway. Findings implicate that VH routing outperforms NRH routing
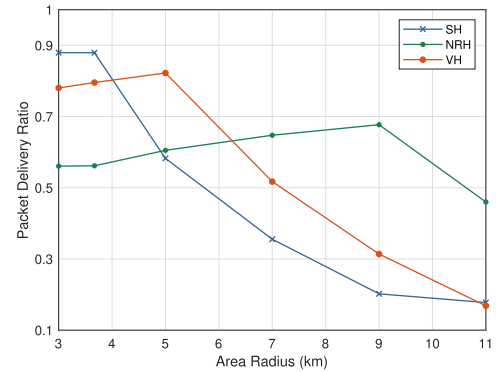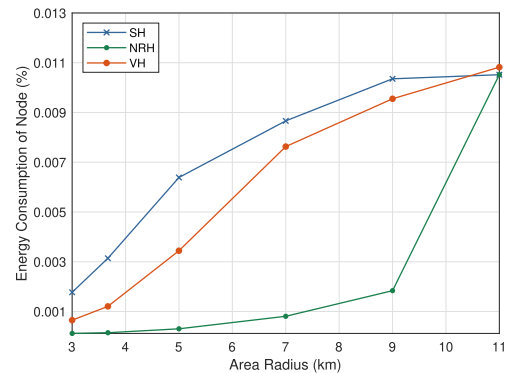
up to about 5 km by providing 80% PDR, about 20% more than NRH routing in this case. Nevertheless, NRH routing performs better than VH routing when the deployment range is increased by more than 6 km.

NRH routing performs better with about 50% more PDR than SH routing and 40% more than VH routing for a 9 km radius. In NRH routing, there are fewer interfering nodes in each node's transmission area since the mean distance between the nodes grows as the area radius is extended. The problem of being unable to access either the intermediate or main gateway is also addressed by NRH routing, which takes into account three virtual rings for coverage radius greater than 9 km.

The average energy consumption of an end node can be observed in Fig. 11. As the system's end nodes are only used for data transmission, energy consumption during packet transmission is calculated in this scenario. Nodes in SH routing consume the most energy since they directly communicate with the main gateway and transmit using more power and current than nodes in other routing schemes. As the area radius is extended, the energy consumption consequently rises. For $A_r = 9$ km, the battery lifetime is almost four times higher in NRH routing than in VH routing.

G. IMPACT OF THE NUMBER OF VIRTUAL RINGS
The impact of the number of virtual rings on PDR and energy consumption can be observed in Fig. 12 and Fig. 13. The
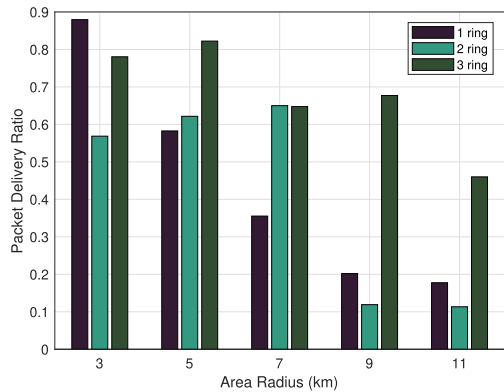
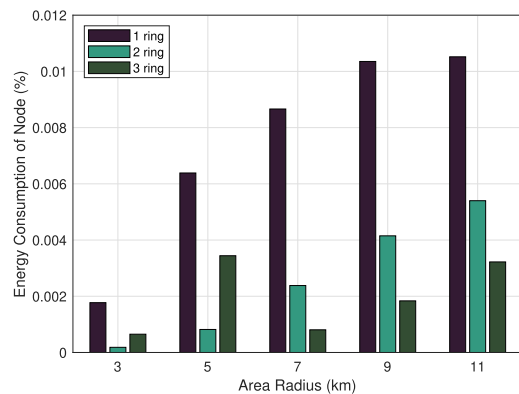**FIGURE 12.** Impact of number of virtual rings on PDR: $N_e = 100$, $TH = 6$, $\Delta_t = [1, 20]$.

FIGURE 13. Impact of number of virtual rings on end node's energy consumption: $N_e = 100$, $TH = 6$, $\Delta_t = [1, 20]$.

FIGURE 14. Intermediate gateway (IG) density: $N_e = 50$, $A_r = 9$ km, $\Delta_t = [1, 20]$.

FIGURE 15. Impact of intermediate gateway (IG) density on PDR: $N_e = 50$, $A_r = 9$ km, $\Delta_t = [1, 20]$.

FIGURE 16. Impact of intermediate gateway (IG) density on PFR: $N_e = 50$, $A_r = 9$ km, $\Delta_t = [1, 20]$.

simulation parameters are: $N_e = 100$, $TH = 6$ and $\Delta_t = [1, 20]$.

Fig. 12 depicts that for a coverage radius beyond 3.67 km, the system with 3 rings outperforms others by providing PDR around 70% up to 9 km. The higher number of rings improves connectivity as the probability of a node finding a forwarding IG increases. For 11 km radius, the system with 3 rings still provides significantly more PDR.

From Fig. 13, it can be observed that the system with 3 rings is more energy efficient compared to others. The battery life of an end node is almost doubled in 3 rings system compared to 2 rings system. The more virtual rings there are in the system, the more likely it is that a node will find a forwarding IG nearby.

H. IMPACT OF INTERMEDIATE GATEWAY DENSITY

In this case, the analysis is performed for a system with 3 rings, 50 nodes, and $A_r = 9$ km. Fig. 14 depicts that as the number of nodes under an IG is reduced, more intermediate gateways are required to support the nodes. It is observed that NRH routing requires more IGs than VH routing.

Fig. 15 shows the impact of IG density in multi-hop LoRaWAN. It is observed that as the number of IGs is reduced for NRH routing, PDR drops significantly. If the number of nodes under an IG is adjusted to 2 instead of 8, it is
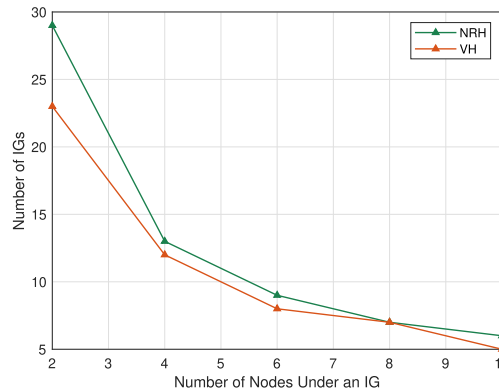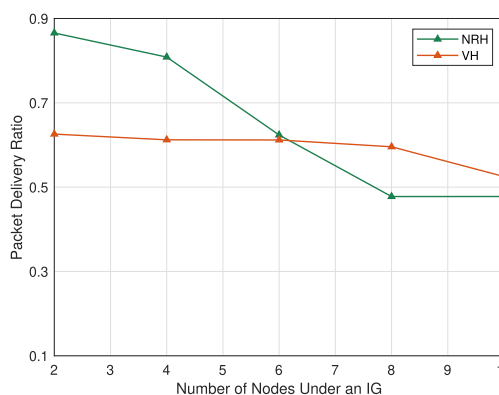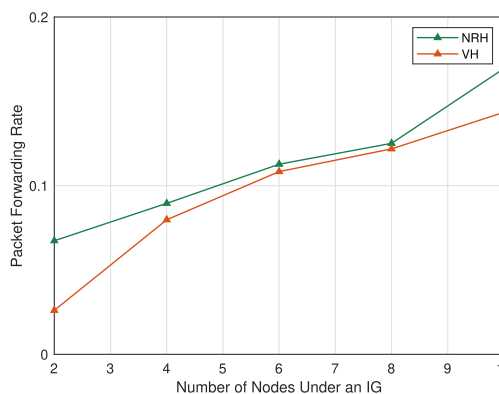
possible to save about 40% of packet loss in NRH routing since additional IGs increase connectivity for the distributed end nodes and enhance PDR. As a result, it directly affects PDR in NRH routing. Due to the employed routing technique, VH routing is less responsive to the variation in IG density.

As additional IGs are deployed to support the end nodes, the packet forwarding rate (packets per second) of an IG decreases, as seen in Fig. 16, suggesting that the likelihood of packet loss due to the occurrence of the same gateway being used at the same time is greatly reduced in the system.
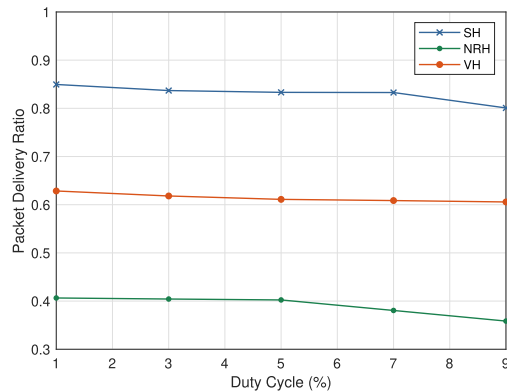
FIGURE 17. Impact of duty cycle variation.

I. IMPACT OF DUTY CYCLE VARIATION

Figure 17 illustrates the impact of duty cycle variation on the system performance. To observe the impact, the simulation parameters are set as: $N_e = 50$, $A_r = 6$ km, $\Delta_t = [1]$, and channel numbers $= 3$. It has been observed that a high duty cycle causes more packets to be sent in the uplink, which increases collisions and eventually lowers PDR.
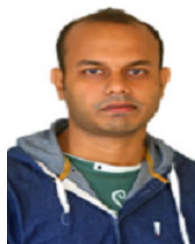
VII. CONCLUSION

The purpose of the paper is to close the performance evaluation gap for multi-hop LoRaWAN. The majority of research is undertaken with highly precise evaluation approaches and has a small number of evaluation criteria. This study offers a comprehensive mathematical framework for analyzing the performance of the suggested multi-hop network from multiple perspectives. Connectivity between devices, the adoption of a distance-based adaptive transmission configuration scheme, and various types of interference were important considerations. According to the investigation, the performance of SH, VH, and NRH routing in terms of packet delivery ratio and energy efficiency varies under different scenarios. Furthermore, it is observed that the intermediate gateway density has a major effect on multi-hop routing since a high IG density guarantees a high level of connection for wide-range deployment. The framework is flexible enough for performance evaluation under various LoRaWAN application scenarios and incorporates pertinent interference issues (i.e., inter-SF, intra-channel, capture effect, timing), environmental impact, and random device deployment.

REFERENCES

[1] M. Centenaro, L. Vangelista, A. Zanella, and M. Zorzi, "Long-range communications in unlicensed bands: The rising stars in the IoT and smart city scenarios," *IEEE Wireless Commun.*, vol. 23, no. 5, pp. 60–67, Oct. 2016.

[2] H. Lee and K. Ke, "Monitoring of large-area IoT sensors using a LoRa wireless mesh network system: Design and evaluation," *IEEE Trans. Instrum. Meas.*, vol. 67, no. 9, pp. 2177–2187, Sep. 2018.

[3] I. F. Priyanta, F. Golatowski, T. Schulz, and D. Timmermann, "Evaluation of LoRa technology for vehicle and asset tracking in smart harbors," in *Proc. IECON 45th Annu. Conf. IEEE Ind. Electron. Soc.*, vol. 1, Oct. 2019, pp. 4221–4228.

[4] J. Haxhibeqiri, I. Moerman, and J. Hoebeke, "LoRa scalability: A simulation model based on interference measurements," *Sensors*, vol. 17, no. 6, p. 1193, May 2017.

[5] M. Rizzi, P. Ferrari, A. Flammini, E. Sisinni, and M. Gidlund, "Using LoRa for industrial wireless networks," in *Proc. IEEE 13th Int. Workshop Factory Commun. Syst. (WFCS)*, May 2017, pp. 1–4.

[6] J. Petäjäjärvi, K. Mikhaylov, R. Yasmin, M. Hämäläinen, and J. Iinatti, "Evaluation of LoRa LPWAN technology for indoor remote health and wellbeing monitoring," *Int. J. Wireless Inf. Netw.*, vol. 24, no. 2, pp. 153–165, Jun. 2017.

[7] A. P. A. Torres, C. B. D. Silva, and H. T. Filho, "An experimental study on the use of LoRa technology in vehicle communication," *IEEE Access*, vol. 9, pp. 26633–26640, 2021.

[8] *Sx1272*, SMTC, Markham, ON, Canada, 2022.

[9] Semtech Corporation. *AN1200.22 LoRa Modulation Basics*. Accessed: Oct. 27, 2022. [Online]. Available: https://www.frugalprototype.com/wp-content/uploads/2016/08/AN1200.22.pdf

[10] N. Sornin, M. Luis, T. Eirich, T. Kramp, and O. Hersent, *LoRaWAN Specification*. San Ramon, CA, USA: LoRa Alliance, 2015.

[11] C. Semtech, "LoRa modem design guide," Semtech Wireless Sens., Camarillo, CA, USA, Tech. Rep. AN1200.13, 2013.

[12] T. Elshabrawy and J. Robert, "Capacity planning of LoRa networks with joint noise-limited and interference-limited coverage considerations," *IEEE Sensors J.*, vol. 19, no. 11, pp. 4340–4348, Jun. 2019.

[13] Semtech Corporation. *Sx1301 Datasheet*. Accessed: Jun. 12, 2022. [Online]. Available: https://www.semtech.com/products/wireless-RF/lora-core/sx1301#documentation

[14] Semtech Corporation. *Sx1272 Datasheet*. Accessed: Jun. 18, 2022. [Online]. Available: https://www.semtech.com/products/wireless-RF/lora-connect/sx1272

[15] *LoRawan-Simple Rate Adaptation Recommended Algorithm*, Semtech Corporation, Camarillo, CA, USA, 2016.

[16] A. Abrardo and A. Pozzebon, "A multi-hop LoRa linear sensor network for the monitoring of underground environments: The case of the medieval aqueducts in Siena, Italy," *Sensors*, vol. 19, no. 2, p. 402, Jan. 2019.

[17] C. Ebi, F. Schaltegger, A. Rüst, and F. Blumensaat, "Synchronous LoRa mesh network to monitor processes in underground infrastructure," *IEEE Access*, vol. 7, pp. 57663–57677, 2019.

[18] D. Lundell, A. Hedberg, C. Nyberg, and E. Fitzgerald, "A routing protocol for LoRa mesh networks," in *Proc. IEEE 19th Int. Symp. World Wireless, Mobile Multimedia Netw. (WoWMoM)*, Jun. 2018, pp. 14–19.

[19] M. Haubro, C. Orfanidis, G. Oikonomou, and X. Fafoutis, "TSCH-over-LoRA : Long range and reliable IPv6 multi-hop networks for the Internet of Things," *Internet Technol. Lett.*, vol. 3, no. 4, Jul. 2020, Art. no. e165.

[20] J. J. L. L. Escobar, F. Gil-Castiñeira, and R. P. D. D. Redondo, "JMAC protocol: A cross-layer multi-hop protocol for LoRa," *Sensors*, vol. 20, no. 23, p. 6893, Dec. 2020.

[21] M. O. Farooq, "Multi-hop communication protocol for LoRa with software-defined networking extension," *Internet Things*, vol. 14, Jun. 2021, Art. no. 100379.

[22] J. R. Cotrim and J. H. Kleinschmidt, "An analytical model for multihop LoRaWAN networks," *Internet Things*, 2023, Art. no. 100807.

[23] S. Barrachina-Muñoz, B. Bellalta, T. Adame, and A. Bel, "Multi-hop communication in the uplink for LPWANs," *Comput. Netw.*, vol. 123, pp. 153–168, Aug. 2017.

[24] A. S. H. Abdul-Qawy and T. Srinivasulu, "SEES: A scalable and energy-efficient scheme for green IoT-based heterogeneous wireless nodes," *J. Ambient Intell. Humanized Comput.*, vol. 10, no. 4, pp. 1571–1596, Apr. 2019.

[25] J. Dias and A. Grilo, "LoRaWAN multi-hop uplink extension," *Proc. Comput. Sci.*, vol. 130, pp. 424–431, Jan. 2018.

[26] S. Barrachina-Muñoz, T. Adame, A. Bel, and B. Bellalta, "Towards energy efficient LPWANs through learning-based multi-hop routing," in *Proc. IEEE 5th World Forum Internet Things (WF-IoT)*, Apr. 2019, pp. 644–649.

[27] G. Zhu, C. Liao, T. Sakdejayont, I. Lai, Y. Narusue, and H. Morikawa, "Improving the capacity of a mesh LoRa network by spreading-factor-based network clustering," *IEEE Access*, vol. 7, pp. 21584–21596, 2019.

[28] C. Liao, G. Zhu, D. Kuwabara, M. Suzuki, and H. Morikawa, "Multi-hop LoRa networks enabled by concurrent transmission," *IEEE Access*, vol. 5, pp. 21430–21446, 2017.

[29] M. Anedda, C. Desogus, M. Murroni, D. D. Giusto, and G. Muntean, "An energy-efficient solution for multi-hop communications in low power wide area networks," in *Proc. IEEE Int. Symp. Broadband Multimedia Syst. Broadcast. (BMSB)*, Jun. 2018, pp. 1–5.

[30] B. Sartori, S. Thielemans, M. Bezunartea, A. Braeken, and K. Steenhaut, "Enabling RPL multihop communications based on LoRa," in *Proc. IEEE 13th Int. Conf. Wireless Mobile Comput., Netw. Commun. (WiMob)*, Oct. 2017, pp. 1–8.

[31] K. Mikhaylov, J. Petaejaejaervi, and T. Haenninen, "Analysis of capacity and scalability of the LoRa low power wide area network technology," in *Proc. Eur. Wireless 22th Eur. Wireless Conf.*, May 2016, pp. 1–6.

[32] M. C. Bor, U. Roedig, T. Voigt, and J. M. Alonso, "Do LoRa low-power wide-area networks scale?" in *Proc. 19th ACM Int. Conf. Modeling, Anal. Simulation Wireless Mobile Syst.*, Nov. 2016, pp. 59–67.

[33] U. Raza, P. Kulkarni, and M. Sooriyabandara, "Low power wide area networks: An overview," *IEEE Commun. Surveys Tuts.*, vol. 19, no. 2, pp. 855–873, 2nd Quart., 2017.

[34] *LoRaWAN 1.1 Specification*, LoRa Alliance, San Ramon, CA, USA, 2017, vol. 11.

[35] F. Adelantado, X. Vilajosana, P. Tuset-Peiro, B. Martinez, J. Melia-Segui, and T. Watteyne, "Understanding the limits of LoRaWAN," *IEEE Commun. Mag.*, vol. 55, no. 9, pp. 34–40, Sep. 2017.

[36] B. Paul, "A novel energy-efficient routing scheme for LoRa networks," *IEEE Sensors J.*, vol. 20, no. 15, pp. 8858–8866, Aug. 2020.

[37] Y. Lalle, M. Fourati, L. C. Fourati, and J. P. Barraca, "Routing strategies for LoRaWAN multi-hop networks: A survey and an SDN-based solution for smart water grid," *IEEE Access*, vol. 9, pp. 168624–168647, 2021.

[38] M. Capuzzo, D. Magrin, and A. Zanella, "Mathematical modeling of LoRa WAN performance with bi-directional traffic," in *Proc. IEEE Global Commun. Conf. (GLOBECOM)*, Dec. 2018, pp. 206–212.

[39] M. DIOP and C. PHAM, "Increased flexibility in long-range IoT deployments with transparent and light-weight 2-hop LoRa approach," in *Proc. Wireless Days (WD)*, Apr. 2019, pp. 1–6.

[40] E. D. Ayele, C. Hakkenberg, J. P. Meijers, K. Zhang, N. Meratnia, and P. J. M. Havinga, "Performance analysis of LoRa radio for an indoor IoT applications," in *Proc. Int. Conf. Internet Things Global Community (IoTGC)*, Jul. 2017, pp. 1–8.

[41] A. Hazmi, J. Rinne, and M. Valkama, "Feasibility study of IEEE 802.11ah radio technology for IoT and M2M use cases," in *Proc. IEEE Globecom workshops*, Dec. 2012, pp. 1687–1692.

[42] M. Hata, "Empirical formula for propagation loss in land mobile radio services," *IEEE Trans. Veh. Technol.*, vol. VT-29, no. 3, pp. 317–325, Aug. 1980.

[43] M. R. Islam, M. Bokhtiar-Al-Zami, B. Paul, R. Palit, J. Grégoire, and S. Islam, "Interference issues in LoRaWAN: A comparative study using simulator and analytical model," in *Proc. IEEE Region 10 Symp. (TENSYMP)*, Jul. 2022, pp. 1–6.

[44] C. Caillouet, M. Heusse, and F. Rousseau, "Optimal SF allocation in LoRaWAN considering physical capture and imperfect orthogonality," in *Proc. IEEE Global Commun. Conf. (GLOBECOM)*, Dec. 2019, pp. 1–6.

[45] M. Slabicki, G. Premsankar, and M. D. Francesco, "Adaptive configuration of LoRa networks for dense IoT deployments," in *Proc. NOMS IEEE/IFIP Netw. Oper. Manage. Symp.*, Apr. 2018, pp. 1–9.

[46] R. Marini, K. Mikhaylov, G. Pasolini, and C. Buratti, "LoRaWANSim: A flexible simulator for LoRaWAN networks," *Sensors*, vol. 21, no. 3, p. 695, Jan. 2021.

MD. RAKIBUL ISLAM received the B.Sc. (Engg.) degree in electrical and electronic engineering from the Shahjalal University of Science and Technology (SUST), Bangladesh, in 2021. He is currently a former member of the IEEE Student Branch, SUST. His research interests include wireless sensor networks, the IoT, and low-power wide-area networks.

MD. BOKHTIAR-AL-ZAMI received the B.Sc. degree in electrical and electronic engineering from the Shahjalal University of Science and Technology, Bangladesh, in 2021. His current research interests include the design and architecture of the Internet of Things, wireless sensor networks, and biosensors.

BISWAJIT PAUL received the B.Sc. degree (summa cum laude) in electronics and telecommunication engineering from North South University, Bangladesh, and the M.Sc. degree from the University of Saskatchewan, Canada. He was the Founder Chairperson of the IEEE Student Branch, NSU. He is currently an Associate Professor with the Department of Electrical and Electronic Engineering, Shahjalal University of Science and Technology (SUST). Before joining SUST, he was a Lecturer with the Department of Electrical and Electronic Engineering, Leading University. So far, he has published a few refereed international journal articles and conference papers. His research interests include wireless sensor systems, cellular networks, wireless enabling technologies, low-power wide area networks, the IoT, 5G/6G, network architecture, communication protocol, and optimization. He also serves as a reviewer for some prestigious journals.

RAJESH PALIT (Member, IEEE) received the Ph.D. degree in electrical and computer engineering from the University of Waterloo, Waterloo, ON, Canada, in 2011. He is currently a Professor with the Department of Electrical and Computer Engineering (ECE), North South University, Bangladesh. He has published more than 50 research papers in refereed international conferences and journals. His research interests include cloud computing and distributed systems, data networking and information security, and ICT for development.

JEAN-CHARLES GRÉGOIRE is currently a Professor with INRS, a constituent of Université du Québec, with a focus on research and education at the master's and Ph.D. levels. His research interest includes telecommunication systems engineering, including protocols, distributed systems, network design and performance analysis, and more recently, security. He also has made significant contributions in the area of formal methods.

SALEKUL ISLAM (Senior Member, IEEE) received the Ph.D. degree from the Computer Science and Software Engineering Department, Concordia University, in 2008. He is currently a Professor and the Head of the CSE Department, United International University, Bangladesh. Previously, he was an FQRNT Postdoctoral Fellow with Énergie, Matériaux et Télécommunications (EMT) Centre, Institut National de la Recherche Scientifique (INRS), Montréal, Canada. His research interests include future internet architecture, blockchain, edge cloud, software-defined networks, multicast security, security protocol validation, machine learning, and AI. He is serving as an Associate Editor for IEEE Access and *Frontiers in High Performance Computing*.

• • •